Phytopathology® • 2023 • 113:1686-1696 • https://doi.org/10.1094/PHYTO-11-22-0428-V

Ecology and Epidemiology

A Compartmental Model for *Xylella fastidiosa* Diseases with Explicit Vector Seasonal Dynamics

Àlex Giménez-Romero,[1,†] Eduardo Moralejo,[2] and Manuel A. Matías[1]

[1] Instituto de Física Interdisciplinar y Sistemas Complejos (IFISC, CSIC-UIB), Campus UIB, 07122 Palma de Mallorca, Spain
[2] Tragsa, Passatge Cala Figuera 6, 07009 Palma de Mallorca, Spain
Accepted for publication 8 February 2023.

Abstract

The bacterium *Xylella fastidiosa* is mainly transmitted by the meadow spittlebug *Philaenus spumarius* in Europe, where it has caused significant economic damage to olive and almond trees. Understanding the factors that determine disease dynamics in pathosystems that share similarities can help to design control strategies focused on minimizing transmission chains. Here, we introduce a compartmental model for *X. fastidiosa*-caused diseases in Europe that accounts for the main relevant epidemiological processes, including the seasonal dynamics of *P. spumarius*. The model was confronted with epidemiological data from the two major outbreaks of *X. fastidiosa* in Europe, the olive quick disease syndrome in Apulia, Italy, caused by the subspecies *pauca*, and the almond leaf scorch disease in Mallorca, Spain, caused by subspecies *multiplex* and *fastidiosa*. Using a Bayesian inference framework, we show how the model successfully reproduces the general field data in both diseases. In a global sensitivity analysis, the vector-to-plant and plant-to-vector transmission rates, together with the vector removal rate, were the most influential parameters in determining the time of the infectious host population peak, the incidence peak, and the final number of dead hosts. We also used our model to check different vector-based control strategies, showing that a joint strategy focused on increasing the rate of vector removal while lowering the number of annual newborn vectors is optimal for disease control.

Keywords: epidemiology, modeling, population biology

Mathematical and computational modeling in ecology and, in particular, epidemiology have been recently recognized as powerful approaches to guide empirical work and provide a framework for the synthesis, analysis, and development of conservation plans and policy-making (Chew et al. 2014; Levin 1992; Murray 1989; Sarkar et al. 2006). Plant epidemics, mainly plant-virus diseases, have often been described by compartmental models, which deal with the overriding importance of transmission mechanisms in determining epidemic dynamics (Jeger et al. 1998, 2004; Madden et al. 2000). These models have contributed to providing answers to some questions related to the ecology of plant diseases and have led to direct applications in disease control while guiding research directions (Jeger and Bragard 2019).

The emergence of vector-borne plant pathogens in new areas causing huge economic impacts, such as *Xylella fastidiosa* and the *Candidatus* Liberibacter spp. (Huanglongbing or citrus greening), has sparked interest in modeling vector-transmitted plant-disease epidemics (Chiyaka et al. 2012; Jeger and Bragard 2019). The vector-borne bacterium *X. fastidiosa* is a multi-host pathogen endemic to the Americas that causes economically important diseases, mostly in woody crops (Hopkins and Purcell 2002). *X. fastidiosa* is a genetically diverse species with three evolutionary well-defined clades forming the *pauca*, *fastidiosa*, and *multiplex* subspecies, native to South, Central, and North America, respectively (Vanhove et al. 2019). Within each subspecies, diverse genetic lineages with different host ranges are found. *X. fastidiosa* is transmitted nonspecifically by xylem-sap-feeding insects belonging to the sharpshooter leafhoppers (Hemiptera: Cicadellidae, Cicadellinae) and spittlebugs (Hemiptera: Cercopoidae) (Redak et al. 2004).

Recently, *X. fastidiosa* has gained renewed interest due to the massive mortality of olive trees in Apulia, Italy (Saponari et al. 2019). The first focus of the olive quick decline syndrome (OQDS) was detected in 2013 around Gallipoli (Apulia, Italy) (Saponari et al. 2013) and since then has spread throughout the region by the meadow spittlebug, *Philaenus spumarius*. Although this was the first official detection of *X. fastidiosa* in Europe, it has recently been demonstrated that the pathogen arrived much earlier in Corsica (Soubeyrand et al. 2018) and in the Balearic islands (Moralejo et al. 2020). Around 1993, two strains of the subspecies *fastidiosa* (ST1) and *multiplex* (ST81) were introduced from California to Mallorca (Spain) with infected almond plants (Moralejo et al. 2020). To date, over 80% of the almond trees in Mallorca show leaf scorch symptoms, and the outbreak has changed the iconic rural landscape of this Mediterranean island (Olmo et al. 2021).

The meadow spittlebug, *P. spumarius* (Hemiptera: Aphrophoridae), has recently been shown to be the main vector of *X. fastidiosa* in Europe, both in transmission experiments and in field studies (Cornara et al. 2017a, 2018b; López-Mercadal et al. 2022; Moralejo et al. 2019; Saponari et al. 2019). *P. spumarius* is a polyphagous species from the Palearctic region, presenting one generation per year (univoltine) and overwintering as eggs. Foam-forming nymphs emerge at the end of winter, feeding on herbaceous plants. The time required for their development to the adult stage depends mainly on temperature and humidity (Bodino et al. 2019; Chmiel and Wilson 1979; Cornara et al. 2018a). In Mediterranean climates, *P. spumarius* adults generally move from the herbaceous cover to the crop canopy as evapotranspiration increases in late spring (May to June). In mid-summer, the populations of *P. spumarius* tend to decrease in the crop canopy, and the insects are captured more

†Corresponding author: À. Giménez-Romero; alex@ifisc.uib-csic.es

Funding: Support was provided through grant PID2021-123723OB-C22 (CYCLE) funded by MCIN/AEI/10.13039/501100011033 and by "ERDF A way of making Europe" and through grant CEX2021-001164-M (María de Maeztu Program for Units of Excellence in R&D) funded by MCIN/AEI/10.13039/501100011033 awarded to À. Giménez-Romero and M. A. Matías.

***e*-Xtra:** Supplementary material is available online.

The author(s) declare no conflict of interest.

frequently in trees and shrubs interspersed in crops. Summer dispersal of spittlebugs to wild hosts as refugees seems to be a common general pattern in Mediterranean crops in Italy (Bodino et al. 2019; Cornara et al. 2021) and Spain (Morente et al. 2018). Because the bacterium has not been detected in spring on insects feeding on the herbaceous cover or in weeds in Europe (Bodino et al. 2019; Cornara et al. 2018a; Olmo et al. 2021), it is assumed that all spittlebug adults acquire the bacteria from the main crop (olive, almond, vine, etc.). Once infected, *X. fastidiosa* colonizes the insect foregut in a persistent and non-circulatory manner without transovarial (parent to offspring) or transstadial (inter-stage) transmission (Almeida and Purcell 2003; Freitag 1951; Purcell and Finlay 1979) and without a period latency after vector acquisition (Almeida and Nunney 1987; Freitag 1951).

Several epidemic models have been already developed for *X. fastidiosa* diseases, but they lack a realistic description of some relevant processes (Jeger and Bragard 2019). Some of these models assume a simple general form for infected host dynamics (Abboud et al. 2019; Daugherty and Almeida 2019; White et al. 2017) or use a simplified S-I compartmental scheme for hosts, disregarding important features such as the latent period or the host mortality rate (Soubeyrand et al. 2018). Models that do take these features into account, however, do not explicitly model the population of vectors responsible for disease transmission (White et al. 2020). Other more recent models have taken a step further in explicitly modeling the vector population (Brunetti et al. 2020; Giménez-Romero et al. 2022b), but the characterization of its dynamics is still relatively simple, as it overlooks the known seasonal patterns of vector abundance. Several recent studies have provided new insights into the ecology and temporal dynamics of the transmission of *X. fastidiosa* by *P. spumarius* in olive plants (Bodino et al. 2019, 2021). However, these experimental data of the pathosystem have not yet been integrated at the population level. Thus, there is a need to continue advancing in the modeling of *X. fastidiosa* diseases by developing more realistic models that can elucidate the fundamental processes involved in vector−host−pathogen interactions and help to design effective control strategies.

In this work, we developed a deterministic continuous-time compartmental model to describe the general epidemiological dynamics of diseases produced by *X. fastidiosa* in Europe. We explicitly account for key biological aspects of the disease, including the seasonal dynamics of its main vector, *P. spumarius*. Our model is able to describe field data from the two major European outbreaks: the OQDS in Apulia, Italy, caused by the subspecies *pauca*, and the almond leaf scorch disease (ALSD) in Mallorca, Spain, caused by subspecies *multiplex* and *fastidiosa*. We aimed to find the most influential parameters in the model with respect to incidence and mortality in both diseases by performing a global sensibility analysis. With this information, the next goal was to explore control strategies acting especially on the vector population.

Materials and Methods

Epidemic model: The SEIR-V model

We developed a deterministic continuous-time compartmental model that incorporates the specific biological features of *X. fastidiosa* diseases in Europe, including the dynamics of the main relevant vector *P. spumarius* (Cavalieri et al. 2019). To build the model, we took the following considerations: (i) We assumed there is no winter recovery of infected hosts, and, thus, they die sometime after infection; (ii) hosts show an asymptomatic period in which they are noninfectious in practice (exposed compartment) because the bacteria are not yet systemically extended (Stevenson et al. 2004; Teviotdale and Connell 2003), whereas vectors are infectious immediately after acquiring the bacterium (Fierro et al. 2019); (iii) vectors have an annual life cycle without mother-to-offspring disease transmission (Freitag 1951; Purcell and Finlay 1979), so we considered the annual emergence of susceptible newborn vectors and a constant death rate for both susceptible and infected vectors; (iv) infected vectors carry the bacterium during their entire lifespan without affecting their fitness; and finally, (v) we did not consider host recruitment or natural death given that the typical development time of *X. fastidiosa* epidemics is faster than the typical host's life cycle.

Altogether, our deterministic continuous-time compartmental model consists of six compartments, four describing the host population (susceptible, S_H, exposed, E_H, infectious, I_H, and removed, R_H), and two describing the vector population (susceptible, S_V, and infected, I_V). The model is defined according to the following processes:

$$\begin{aligned} &S_H + I_V \xrightarrow{\beta} E_H + I_V,\ E_H \xrightarrow{\kappa} I_H,\ I_H \xrightarrow{\gamma} R_H \\ &S_V + I_H \xrightarrow{\alpha} I_V + I_H,\ S_V \xrightarrow{\mu} \emptyset,\ I_V \xrightarrow{\mu} \emptyset \end{aligned} \tag{1}$$

which are illustrated in Figure 1, being the birth of new susceptible vectors described as a source term. Thus, the host-vector compartmental model is written as

$$\begin{aligned} \dot{S}_H &= -\beta S_H I_v / N_H \\ \dot{E}_H &= \beta S_H I_v / N_H - \kappa E_H \\ \dot{I}_H &= \kappa E_H - \gamma I_H \\ \dot{R}_H &= \gamma I_H \\ \dot{S}_v &= N_v(0) \sum_{n=1}^{\infty} \delta(t - nT) - \alpha S_v I_H / N_H - \mu S_v \\ \dot{I}_v &= \alpha S_v I_H / N_H - \mu I_v \end{aligned} \tag{2}$$

The model describes the exposure of susceptible hosts, S_H, at a rate β through their interaction with infected vectors, I_v, whereas susceptible vectors, S_v, get infected immediately at a rate α through their interaction with infectious hosts I_H. Exposed hosts get infectious at rate κ, being the mean latent period $\tau_E = 1/\kappa$, whereas infectious hosts die at rate γ, having a mean infectious period of $\tau_I = 1/\gamma$. Infected vectors stay infected and infectious for the rest of their lifetime. Regarding the seasonal dynamics of vectors, we assume that new adults emerge synchronously each year in fields being all susceptible. This is represented by the term $N_v(0)\sum_{n=1}^{\infty}\delta(t-nT)$ in equation 2, where $T = 1$ year is the period and $\delta(t - nT)$ is Dirac delta function and basically implements a yearly pulse of new vectors at a certain moment in the year. Vectors are removed (die, move to herbaceous vegetation and other non-host trees, exit the field, etc.)

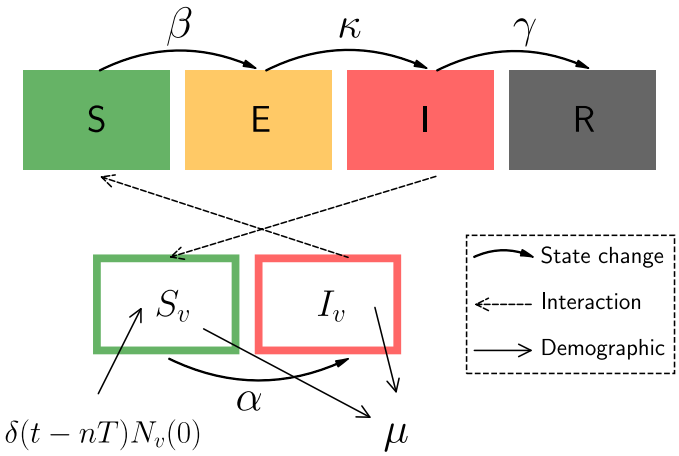

Fig. 1. Schematic representation of the model equation 2. Boxes are the compartments in which the population is divided, solid curved arrows represent changes in state (i.e., transitions between compartments), dashed arrows depict the crossed interaction between hosts and vectors, and solid straight arrows represent demographic changes in vector population.

at a given rate μ, which we consider identical for susceptible and infected vectors. For simplicity, we consider that the quantity of annual newborn adults, $N_v(0)$, is constant. This outburst of new adults followed by an exponential decay resembles the temporal patterns on the abundance of *P. spumarius* observed in crop fields (Antonatos et al. 2021; Beal et al. 2021; Cornara et al. 2017a; López-Mercadal et al. 2021) (Supplementary Fig. S1).

In our model (equation 2) the crossed nonlinear terms in $\dot{S}_H$ and $\dot{S}_v$, $S_H I_v$, and $S_v I_H$ are divided by the total host population, N_H. Thus, the vector-to-plant infection process is modeled using mass action incidence, which is density dependent, whereas the plant-to-vector infection process is modeled using standard incidence, which is frequency dependent (Martcheva 2015). This implies that doubling the number of vectors in the crop field would double the number of resulting exposed (or infected) hosts, as this process is population-dependent (mass action incidence), whereas doubling the number of hosts would not result in more vectors per unit area being infected, as this process only depends on the contact probability, being frequency dependent (standard incidence). We think this is the most reasonable assumption because, for a given plantation framework, increasing the number of hosts is expected to also increase the area of the field, whereas the number of vectors is an independent quantity.

Basic reproductive number

The basic reproductive number, R_0, of the model cannot be trivially computed using standard methods, such as the next-generation matrix (Diekmann et al. 2010), as there is no pre-pandemic fixed point in the system of differential equations (equation 2). For periodically varying vector populations, rigorous methods have been developed (Bacaër 2007), but not for the case of growing or decaying vector populations. Here, we use the simple method developed in the work of Giménez-Romero et al. (2022a) (see Appendix II), which effectively computes the average number of secondary infections produced by an initially infectious individual in one generation. Thus, the effective basic reproductive number is given by

$$R_0 = \frac{\beta\alpha}{\mu\gamma}\frac{S_H(0)}{N_H^2}\frac{N_v(0)}{\mu\tau}\left(1 - e^{-\mu\tau}\right) \tag{3}$$

where τ corresponds to the time length of one generation, in our case 1 year. This R_0 is calculated using the initial susceptible host population, $S_H(0)$. Below, we also use a time-dependent $R_0(t)$ using $S_H(t)$.

Epidemiological data

Epidemiological data from an ALSD outbreak on the island of Mallorca, Balearic Islands, Spain, were taken from Moralejo et al. (2020). Dated phylogenetic analysis and estimates of disease incidence showed that the introduction of both subspecies occurred around 1993, and 79% almond trees were infected in 2017 (Moralejo et al. 2020). The annual proportion of infected individuals in the almond tree population between 1993 and 2017 was estimated by analyzing through qPCR the presence of *X. fastidiosa* DNA in the growth rings of 34 sampled trees (cf. Fig. 3 in Moralejo et al. 2020). The disease progression curve was estimated without distinguishing whether infections were caused by *multiplex* or *fastidiosa* subspecies. In addition, a two-sided bootstrap confidence interval for each data point was set using the SciPy bootstrap function in Python (Virtanen et al. 2020). On the other hand, epidemic data for OQDS were retrieved from (White et al. 2020). The data consisted of two to three yearly censuses of symptom prevalence in 17 olive groves infected with *X. fastidiosa* subsp. *pauca* in Apulia, Italy, which were aggregated to fit our model as shown in Figure 4 in White et al. (2020). Because the compartments of our model are not in one-to-one correspondence with those shown in the work of White et al. (2020), we used the sum of the symptomatic and desiccated infected trees in the dataset ($I_S + I_D$) to fit the sum of the infected and dead trees ($I + R$) and the sum of susceptible and asymptomatic hosts ($S + I_A$) to fit the sum of susceptible and exposed hosts ($S + E$). The processed data used to fit the model can be found in Giménez-Romero (2022), and the raw data can be found in the supplementary data accessible online of the cited articles Moralejo et al. (2020) and White et al. (2020).

Model fitting through Bayesian inference

We employed an informative normal $\mathcal{N}(\hat{\mu}, \hat{\sigma}^2)$ prior distribution, with $\hat{\mu}$ and σ, the mean and standard deviation, respectively, for previously measured parameters in the literature, such as the infectious and latent periods for ALSD, $\tau_I \sim \mathcal{N}(14, 4)$, $\tau_E \sim \mathcal{N}(4, 1)$ (Moralejo et al. 2020; Teviotdale and Connell 2003) and OQDS, $\tau_I \sim \mathcal{N}(3.5, 1)$, $\tau_E \sim \mathcal{N}(1.75, 0.5)$ (Fierro et al. 2019). The corresponding rates are given by $\gamma = 1/\tau_I$ and $\kappa = 1/\tau_E$, respectively. Similarly, a prior normal distribution was used for the removal rate of vectors, $\mu \sim \mathcal{N}(0.02, 0.0075)$, as the mean value $\mu = 0.02$ already captures the vector dynamics observed in field data (Supplementary Fig. S1). Regarding the prior distribution for the transmission rates, a very wide and uninformative uniform prior distribution, $\beta \sim \mathcal{U}(0.001, 1)$ and $\alpha \sim \mathcal{U}(0.001, 1)$, was used for each parameter. The number of hosts, N_H, was already provided in the datasets, but, given the lack of information about the vector population, we assumed $N_v(0) = N_H/2$ for the initial vector population of each year. However, we tested the robustness of our results by changing $N_v(0)$.

The posterior distributions of the parameters were approximated using the Markov chain Monte Carlo algorithm No U-Turn Sampler (NUTS) with the recommended target acceptance rate of 65% (Homan and Gelman 2014). To ensure a proper convergence, we constructed three independent Markov chains with 10^5 iterations each after a burn-in of 10^4 iterations and checked that the results were statistically equivalent. For each chain, we started at the maximum-likelihood parameters yielded by the Nelder-Mead algorithm with 1,000 iterations.

The parameters of our compartmental model were determined by fitting the model to data by means of a Bayesian inference framework using the Turing.jl package (Ge et al. 2018) in Julia (Bezanson et al. 2017). The scripts used to fit the model can be found in Giménez-Romero (2022).

Sensitivity analysis

We performed a global sensitivity analysis (GSA) (Saltelli et al. 2004) of the model to assess the relative contribution of its parameters and their interactions with different features of the epidemic. In contrast to a local sensitivity analysis (LSA), a GSA assesses the influence of a large domain of the parameter space in the desired outputs of the model. We performed GSA by means of a variance-based analysis, the Sobol method (Sobol 2001). This particular method provides information not only on how a particular parameter alone influences the model outputs (as happens with LSA), but also due to the nonlinear interactions among two or more parameters. Briefly, the method considers the model output, Y, as a general function of the inputs, $f(x_1, ..., x_n)$, so that the variance of the output, $Var(Y)$ is decomposed as the sum of the variances given by the variations of the parameters alone and its interactions,

$$Var(Y) = \sum_{i=1}^{n} Var(f(x_i)) + \sum_{i<j}^{n} Var(f(x_i, x_j)) + \cdots$$

This information is organized in what are known as Sobol indices. The total order indices are a measure of the total variance of the output quantity caused by variations of the input parameter and its interactions, $S_T = Var(f(x_1, ..., x_n))/Var(Y)$. First-order (or "main effect") indices are a measure of the contribution to the output variance given by the variation of the parameter alone but averaged over the variations in other input parameters, $S_i = Var(f(x_i))/Var(Y)$. Second-order indices consider first-order interactions between parameters, $S_{ij} = Var(f(x_i, x_j))/Var(Y)$. Further indices can be

obtained describing the influence of higher-order interactions between parameters, but these are not going to be considered.

Following the Sobol method, we analyzed the variation of the time at which the infectious population peaks, t_{peak}, the magnitude of this peak, I_{peak} and the final number of dead hosts, R_∞, relative to variations of the model parameters. The method was implemented within the Julia high-level programming language (Bezanson et al. 2017) using the sub-package DiffEqSensitivity.jl in the DifferentialEquations.jl package (Rackauckas and Nie 2017).

Results

Model fit and parameter estimates

The posterior distributions of the fitted parameters, including their estimated mean and median for ALSD and OQDS, are shown in Figures 2 and 3, respectively, together with the assumed prior distributions. We observe that the literature-driven priors for the latent and infectious period, τ_E and τ_I, were already very good guesses and changed slightly, converging to the appropriate distribution that better fitted the epidemic data for both ALSD and OQDS (Figs. 2A and B and 3A and B). Similarly, the prior for the vector removal rate, μ, obtained from field data, was good enough so that little changes were needed for convergence (Figs. 2C and 3C). On the other hand, we also observe that the completely uninformative priors for the transmission rates successfully converged to the posterior distributions (Figs. 2D and E and 3D and E).

The latter distributions are far from a Gaussian-like shape (note that the x axis is log-scaled), being heavy-tailed. This kind of distribution highly distorts the statistical measures of mean, median, and standard error, indicating that the estimates for transmission rates are not as robust as the estimates for the other parameters. These rather uninformative distributions most probably arise because of the lack of data about the vector, that is, $S_v(t)$ and $I_v(t)$, to constrain the fits. In essence, many combinations of α and β can similarly fit the host data while yielding quite different time series for $S_v(t)$ and $I_v(t)$, which cannot be contrasted due to the lack of field data. Nevertheless, the obtained best-fit mean and median parameters, although quite different, are able to perfectly fit the data (Fig. 4). Finally, we also observe that the variance for the field data also converged to a bell-shaped distribution.

Mean and median parameter estimates (i.e., the best-fit parameter values for ALSD and OQDS) are summarized in Tables 1 and 2, respectively. As already seen from the posterior distributions, the best-fit values for τ_E, τ_I, and μ are close to the ones given by literature and field data for both diseases. Conversely, α and β are rather uninformative, as their 95% confidence intervals cover almost two orders of magnitude. This again indicates that without some data about the evolution of the vector states in time, $S_v(t)$ and $I_v(t)$, it is nearly impossible to derive the proper values for these parameters.

Overall, the data fall within the 99% confidence limits of the fitted model for both the ALSD and OQDS outbreaks (Fig. 4B and D). We also computed the instantaneous reproductive number, $R_0(t)$, by using equation 3 with $S_H(t)$ instead of only $S_H(0)$ along the simulation. Notably, $R_0(t) = 1$ coincides with the stopping of new infections being produced; that is, the number of exposed hosts does not increase (Fig. 4A to C). This supports our approximate method for computing the reproductive number for *X. fastidiosa* diseases (Appendix II, equation iii). Due to the different time scales of both epidemics ($\tau_I^{ALSD} + \tau_E^{ALSD} > \tau_I^{OQDS} + \tau_E^{OQDS}$), the OQDS outbreak dies out earlier than the one for ALSD.

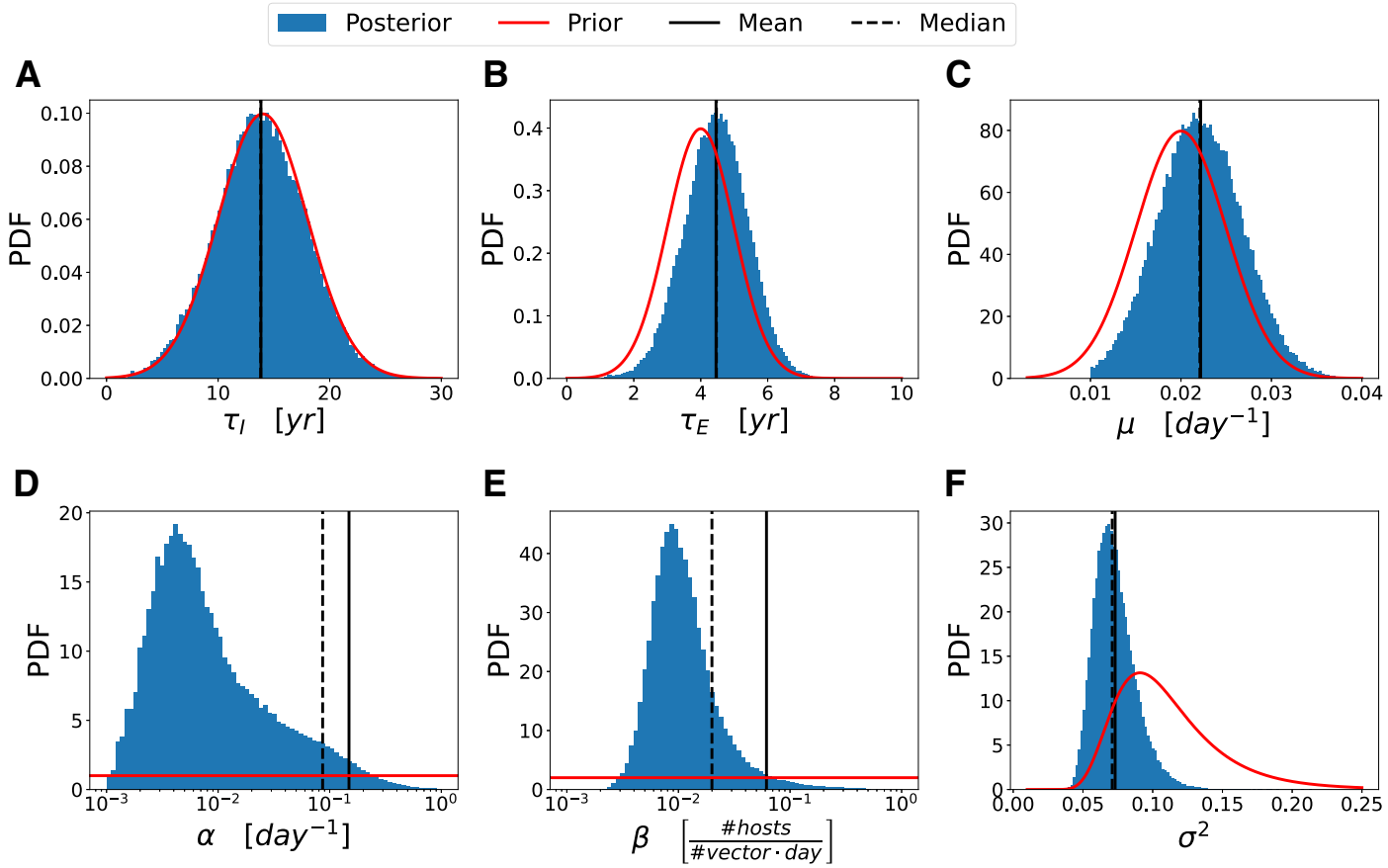

Fig. 2. Posterior (blue histograms) and prior (red line) distributions of the model parameters for almond leaf scorch disease. Solid and dashed black lines correspond to the mean and median of the posterior distributions. **A,** Host infectious period $\tau_I = 1/\gamma$. **B,** Host latent period $\tau_E = 1/\kappa$. **C,** Vector removal rate μ. **D,** Vector infection rate α. **E,** Host infection rate β. **F,** The variance of the field data σ^2.

We notice that for ALSD, a large proportion of the vector population gets infected every year (Fig. 4A), whereas a very small proportion is needed in OQDS to produce a lethal outbreak (Fig. 4C). However, this last statement is rather unrealistic, as around 50% of the vectors that are captured in Apulia are indeed infected by *X. fastidiosa* (Cavalieri et al. 2019; Cornara et al. 2017b). Thus, the evolution of the infected vector population should be qualitatively similar to that obtained for ALSD (Fig. 4C). As previously explained, different suitable combinations of α and β parameters should give rise to similar progression curves for the hosts and different ones for the vectors, but the realistic values for these parameters cannot be obtained from the Bayesian fit due to the lack of data of the vector states, $S_v(t)$, $I_v(t)$.

Nevertheless, by manually exploring other values for α and β parameters, we can obtain a more biologically plausible scenario for the OQDS that is still able to fit the available data for the hosts. Figure 5A shows a simulation of the model with previously inferred best-fit median parameters for OQDS. By changing the values of α and β, we obtain a more realistic scenario in which around a 50% of the vector population getting infected during the outbreak (Fig. 5B) (Cavalieri et al. 2019; Cornara et al. 2017b). Noteworthy, the β value obtained in this way is almost identical to the transmission rate recently reported by Bodino et al. (2021) for OQDS. This change in the transmission parameters only affects the progression curve of the infected vector population, the progression of the host compartments being practically unchanged (Fig. 5C). Anyway, both sets of parameter values for α and β can properly fit the field data, corresponding exclusively to the host population (Fig. 5D).

The model adjusted to the progression curves of both diseases indicates that the transmission rate α must be greater than β when the proportion of infected vectors is relatively high (>30%). We checked if the relationship between α and β held when changing the assumed $N_v(0) = N_H/2$, obtaining that it kept approximately the same for very different values of the initial vector population.

Global sensitivity analysis

We computed the sensitivity indices for the model parameters with respect to the more relevant quantities of interest, namely, the time at which the number of infectious hosts is maximal, t_{peak}, the maximum number of infectious hosts, I_{peak} and the final number of dead hosts, R_∞. The results were obtained exploring

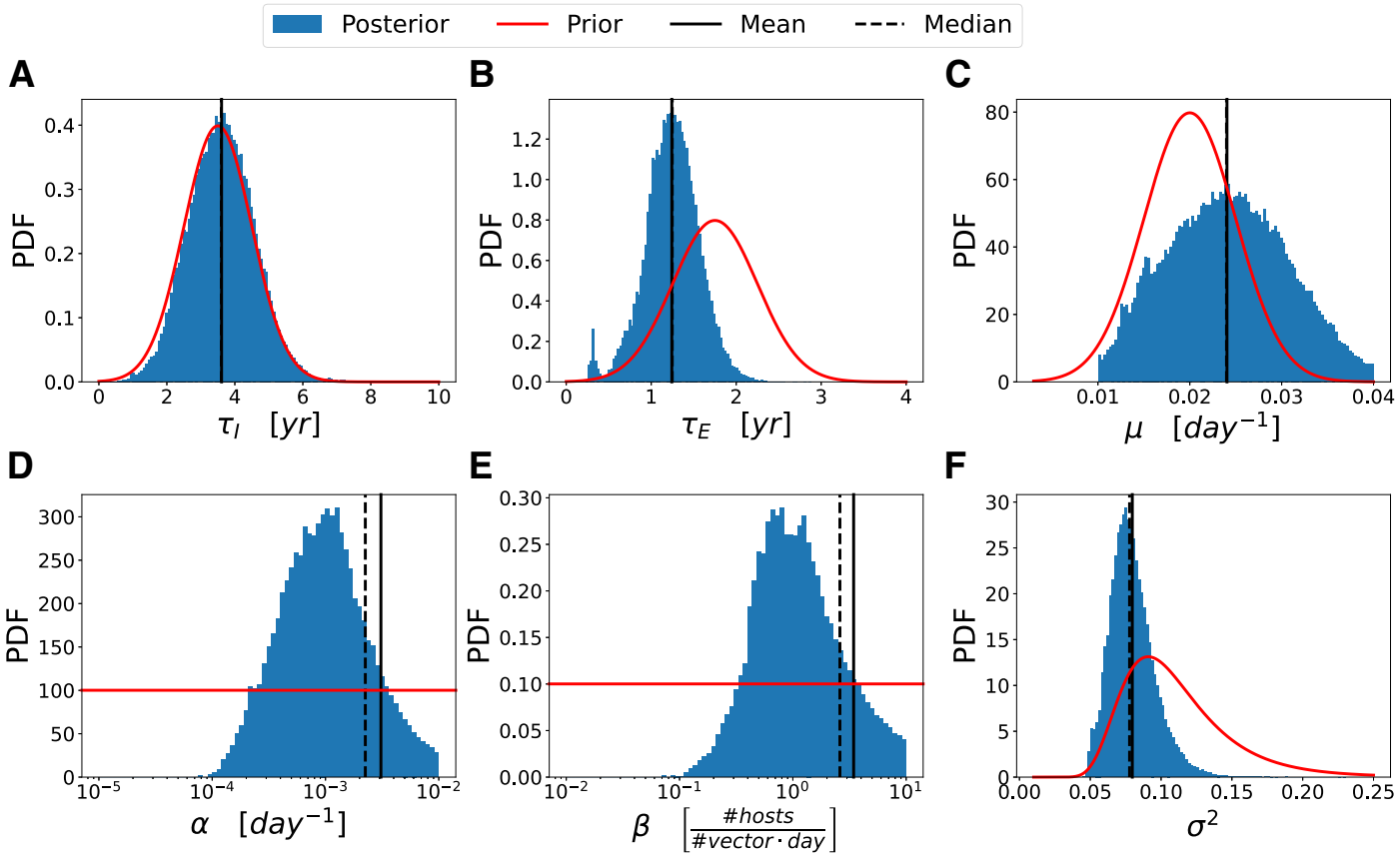

Fig. 3. Posterior (blue histograms) and prior (red line) distributions of the model parameters for olive quick decline syndrome (OQDS). Solid and dashed black lines correspond to the mean and median of the posterior distributions. **A,** Host infectious period $\tau_I = 1/\gamma$. **B,** Host latent period $\tau_E = 1/\kappa$. **C,** Vector removal rate μ. **D,** Vector infection rate α. **E,** Host infection rate β. **F,** Variance of the field data σ^2.

TABLE 1. Estimated epidemiological parameters from Bayesian model fitting to the disease progression curve of almond leaf scorch disease in Mallorca

Parameter	Definition	Units	Posterior mean	Posterior median	95% confidence interval
τ_I	Host infectious period	Year	13.84	13.82	[7.12, 20.47]
τ_E	Host latent period	Year	4.46	4.47	[2.88, 5.99]
β	Host infection rate	$\frac{\#hosts}{\#vector \cdot day}$	0.062	0.02	[0.0061, 0.3013]
α	Vector infection rate	Day^{-1}	0.15	0.086	[0.0047, 0.54]
μ	Vector removal rate	Day^{-1}	0.0222	0.0221	[0.015, 0.030]
R_0	Basic reproductive number	–	133	25	–

the parameter space constrained to the intervals $\{\beta \in (0.001, 0.1), \tau_E \in (3, 7), \tau_I \in (5, 25), \alpha \in (0.001, 1), \mu \in (0.01, 0.04)\}$ using 10^4 Quasi-Monte Carlo samples and are summarized in Figure 6.

Parameters α, β, and μ are the most influential with regard to the time at which the infectious host population peaks, t_{peak}, the magnitude of the peak, I_{peak}, and the final number of dead hosts, R_∞. The total output variance (total order indices) cannot be explained by the variances of the parameters alone (first-order indices) (Fig. 6). Therefore, higher-order interactions among the parameters importantly affect the sensitivity of the quantities under study. Indeed, the contribution to the total output variance of γ and κ for t_{peak} and R_∞ come notably from higher-order interactions. This can be checked in panels B, D, and F of Figure 6, in which the contribution to the output variance from interactions between pairs of parameters (second-order indices) is represented. Interactions among the parameters contribute to increasing the output variance with respect to t_{peak} and I_{peak}, whereas the effect is more heterogeneous in the case of R_∞. In particular, the interactions between $\alpha - \beta$ and $\alpha - \mu$ produce the main contributions to the increase of output variance in all cases, whereas $\kappa - \beta$, $\kappa - \alpha$ and $\kappa - \mu$ interactions decrease the output variance.

Epidemic control through vector management

The sensitivity analysis clearly indicates that acting on α, β, and μ is the best strategy to lower disease incidence and mortality. However, controlling transmission rates is cumbersome, so a different control strategy based only on vector control is considered in this section. In our model, there are two ways of implementing vector-population control: (i) decreasing the typical time, $1/\mu$, that vectors spend between crops each year by some mechanism (thus increasing μ) and (ii) reducing the initial number of vectors that invade crops each year (e.g., lowering $N_v(0)$ via egg or nymph control) (Lago et al. 2023).

We analyzed the effect of vector management by simulating epidemic outbreaks using different values of μ and $N_v(0)$ and keeping the rest of parameters as fitted for both ALSD and OQDS outbreaks (Fig. 7). In both epidemics, decreasing the presence time, as well as the number of vectors, contributes to controlling the epidemic by lowering R_0 and, consequently, the final size of the epidemic, R_∞. Furthermore, we observe that decreasing vector presence is more efficient than decreasing its annual initial population; that is, we further reduce R_∞, the final size of the epidemic, by applying a similar reduction in the residence time $1/\mu$. This could also be anticipated

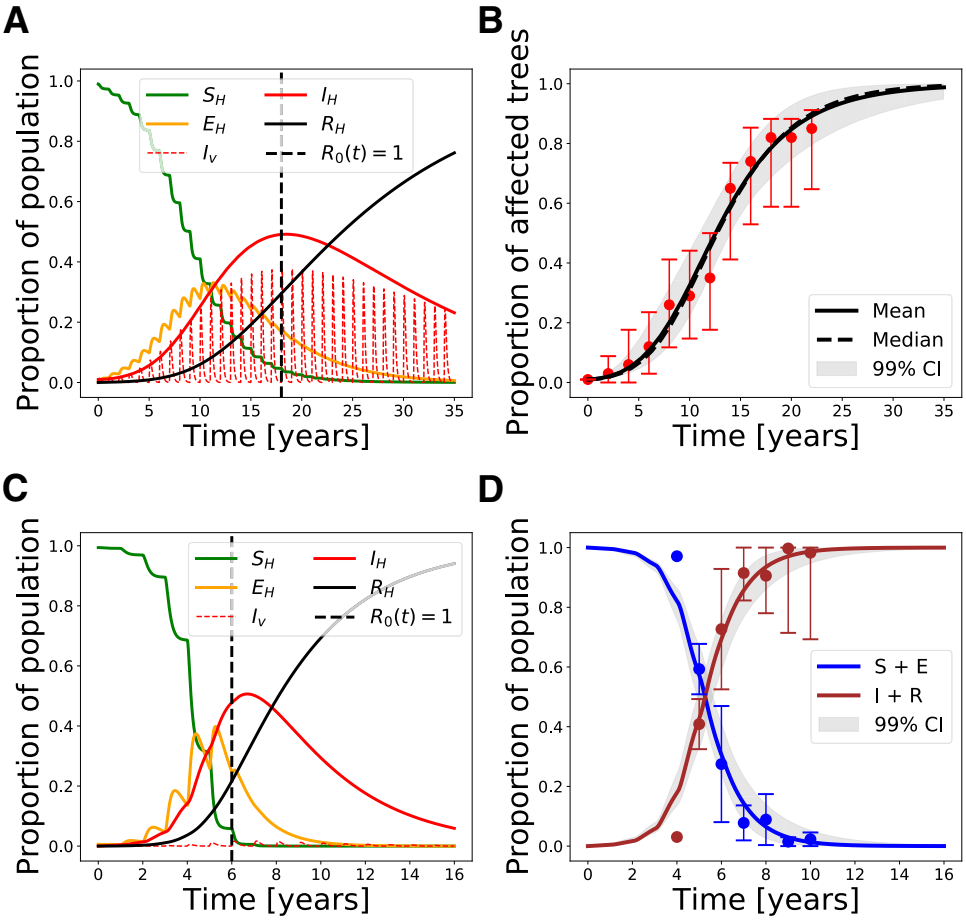

Fig. 4. A, Simulation of the model with the best-fit parameters for almond leaf scorch disease (ALSD). **B,** Model fit to field data by means of the mean and median values of the posterior distributions of the parameters for ALSD. **C,** Simulation of the model with the best-fit parameters for olive quick decline syndrome (OQDS). **D,** Model fit to field data by means of the mean and median values of the posterior distributions of the parameters for OQDS. The gray-shaded area corresponds to the 99% confidence interval. The error bars for the field data correspond to their 95% confidence intervals obtained with a bootstrapping technique.

TABLE 2. Estimated epidemiological parameters from Bayesian model fitting to the disease progression curve of olive quick decline syndrome in Apulia

Parameter	Definition	Units	Posterior mean	Posterior median	95% confidence interval
τ_I	Host infectious period	Year	3.61	3.60	[2.06, 5.20]
τ_E	Host latent period	Year	1.24	1.25	[0.70, 1.75]
β	Host infection rate	$\frac{\#hosts}{\#vector \cdot day}$	3.44	2.60	[0.55, 8.79]
α	Vector infection rate	Day^{-1}	0.0031	0.0022	[0.0005, 0.0084]
μ	Vector removal rate	Day^{-1}	0.0240	0.0240	[0.014, 0.035]
R_0	Basic reproductive number	–	33	21	–

as R_0 depending quadratically on $1/\mu$ but only linearly on $N_v(0)$ (equation 3). However, the minimal intervention strategy, starting from the current situation in the $(1/\tau, N_v(0))$ parameter space that yields an absolute control of the epidemic, $R_0 < 1$, involves a mixed strategy of lowering both $1/\mu$ and $N_v(0)$.

Discussion

In this work, we developed a deterministic continuous-time compartmental model for *X. fastidiosa* vector-borne diseases in Europe. The model attempts to characterize the main biotic processes that lead to the development of epidemics, including the seasonal dynamics of the main vector, *P. spumarius*. We show how the model is sufficiently general to represent with some accuracy the parameters that determine the ALSD in Mallorca (Spain) and the OQDS in Apulia (Italy), both transmitted by *P. spumarius*. To our best knowledge, this is the first mathematical model describing *X. fastidiosa* epidemics that considers the temporal pattern of vector abundance observed in field data, faithfully representing the known biological information about the pathosystem. It includes a dynamic approximation of the non-stationary populations of *P. spumarius*, mathematically represented by a sporadic source term through which vectors are born every year, and an exponential decay term. Due to the non-stationarity of the vector dynamics, R_0 in the model cannot be computed with standard methods such as the next-generation matrix (Diekmann et al. 2010). To circumvent this problem, we applied an approximate method to compute it as previously proposed by (Giménez-Romero et al. 2022a). We show that this approximate R_0 correctly characterizes the epidemic, further validating the method proposed by Giménez-Romero et al. (2022a).

Nonlinear mathematical models of disease transmission enhance our understanding of the different mechanisms operating in an epidemic, especially compared with correlative or machine learning methods, often very useful in practice but offering very little understanding. A key aspect to render these models useful is the determination of the parameters from available data. If this step can be properly performed, these models become very predictive and especially helpful to design disease control strategies. However, an appropriate calibration of the model relies on access to good-quality field data, which is often the bottleneck for the application of this kind of model. In the present study, the parameters were obtained using a Bayesian inference framework, which relies on probability distributions rather than point-like measures. This way, mean or median values can be considered together with their confidence intervals able to characterize the robustness of the obtained parameters. In general, we obtained different values of the parameters for the ALSD and OQDS outbreaks in Mallorca and Apulia, respectively. The fitted values, however, are in good agreement with previous field-based measures for each disease, whereas the differences observed between both outbreaks may reflect differences between the *X. fastidiosa* subspecies and crops involved (deciduous versus evergreen).

One of the conclusions of the study is that the available data for both diseases is not enough to obtain robust estimates for all of the model parameters. The lack of data about the vector population compartments yields many possible values for the parameters that regulate transmission, α and β, provided that the progression of the host compartments correctly fits the field data. In other words, very infectious vectors (high β) that hardly ever get infected (low α) can produce a similar outbreak within the host population to that produced by very low infectious vectors (low β) that get infected very often (high α). The great difference in these situations would be

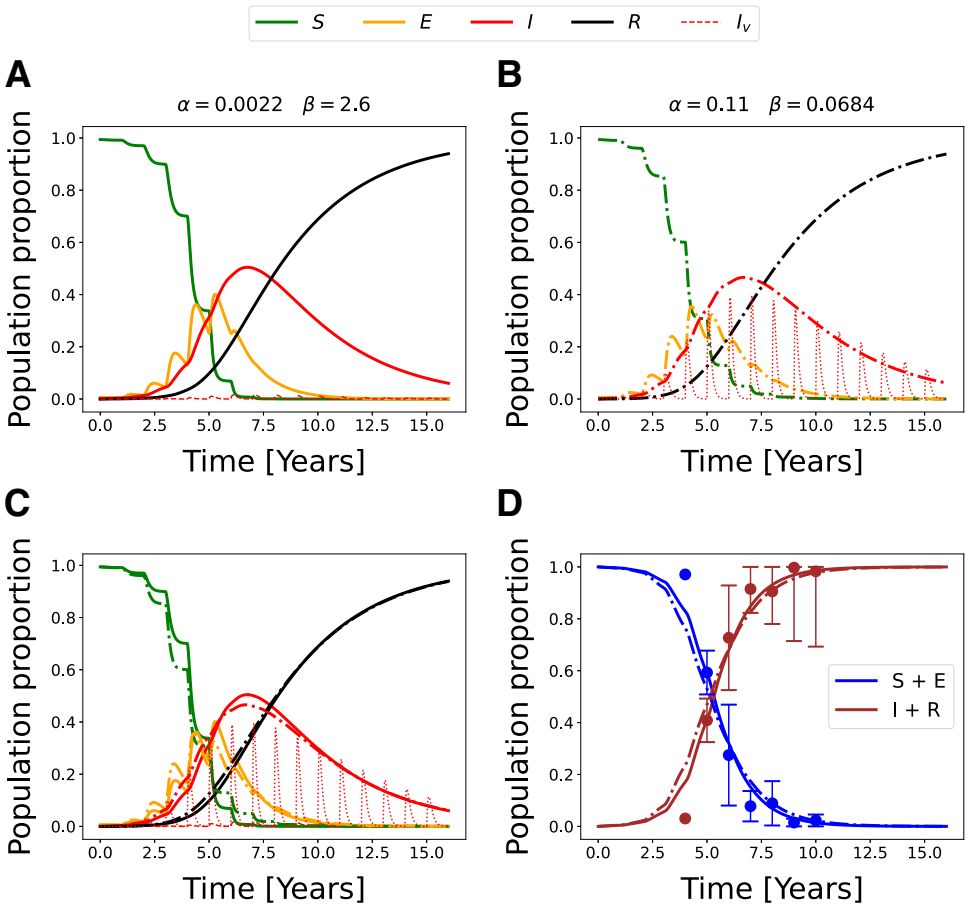

Fig. 5. A, Simulation of the model with the original best-fit parameters for olive quick decline syndrome (OQDS). **B,** Simulation of the model with the original best-fit parameters for OQDS but with different α, β values. **C,** Comparison of the progression curves. Note that the curves for the hosts are very similar, whereas the curve for the infected vector population is very different. **D,** Comparison of the model fit to the data with both simulations. Solid lines correspond to results with the original best-fit parameters, whereas dash-dot lines correspond to the results of the more realistic scenario with different α and β values.

that, in the former, the infected vector population would be very low, whereas in the latter, it would be quite high. This is a manifestation of parameter unidentifiability from the fit (Chowell 2017; Roosa and Chowell 2019), which stresses the importance of transmission and calls for detailed measurements of the vector population, and not just of the hosts. Furthermore, to compare transmission rates between different diseases caused by *X. fastidiosa* (e.g., β, α), it is necessary to know the vector-host population ratio of the pathosystem (N_v/N_H) because β is expressed as a number of hosts per vectors per day. Although, in general, populations of *P. spumarius* in the canopy of olive trees are much larger than those found in the almond trees of the Balearic Islands during the months of July and August (López-Mercadal et al. 2021), our work is based on data from studies in which information of the vector populations is not provided. Without this information, therefore, conclusive results regarding transmission cannot be obtained.

In any case, our model shows that the vector-to-plant transmission process, mediated by β, is somehow different from that from the plant-to-vector one, mediated by α. In essence, β must be smaller than α in order to reproduce the observed outbreaks and have a sufficiently large vector population getting infectious, this fact being independent of the particular choice of $N_v(0)/N_H$. This heterogeneity can be caused by several factors: differences in the efficiency of plant-to-vector transmission with respect to vector-to-plant transmission, differences in contact rates (i.e., susceptible vectors contact trees at a different rate than infected vectors), vector feeding preferences (i.e., differences in the probability of contacting a susceptible host compared to an infectious host), and so on. Indeed, our mathematical model assumes constant contact rates with no preferences over any host state, so that under these assumptions, it indicates that the probability of effectively transmitting the pathogen from plant to vector is greater than from vector to plant.

However, this interpretation is subject to this particular assumption, so that to fully disentangle this question, experimental work in the form of transmission assays should be performed. Furthermore, we found that the timing and magnitude of the infectious host peak and the final number of dead hosts are mostly controlled by the vector-to-plant transmission rate, β, the plant-to-vector transmission rate, α, and the vector removal rate, μ. Because these parameters are strongly related to the vector, the analysis makes clear that enhancing the knowledge about the vector, as well as obtaining precise data, is crucial to improve the modeling of *X. fastidiosa* diseases and poses important questions to be solved in specifically designed experiments.

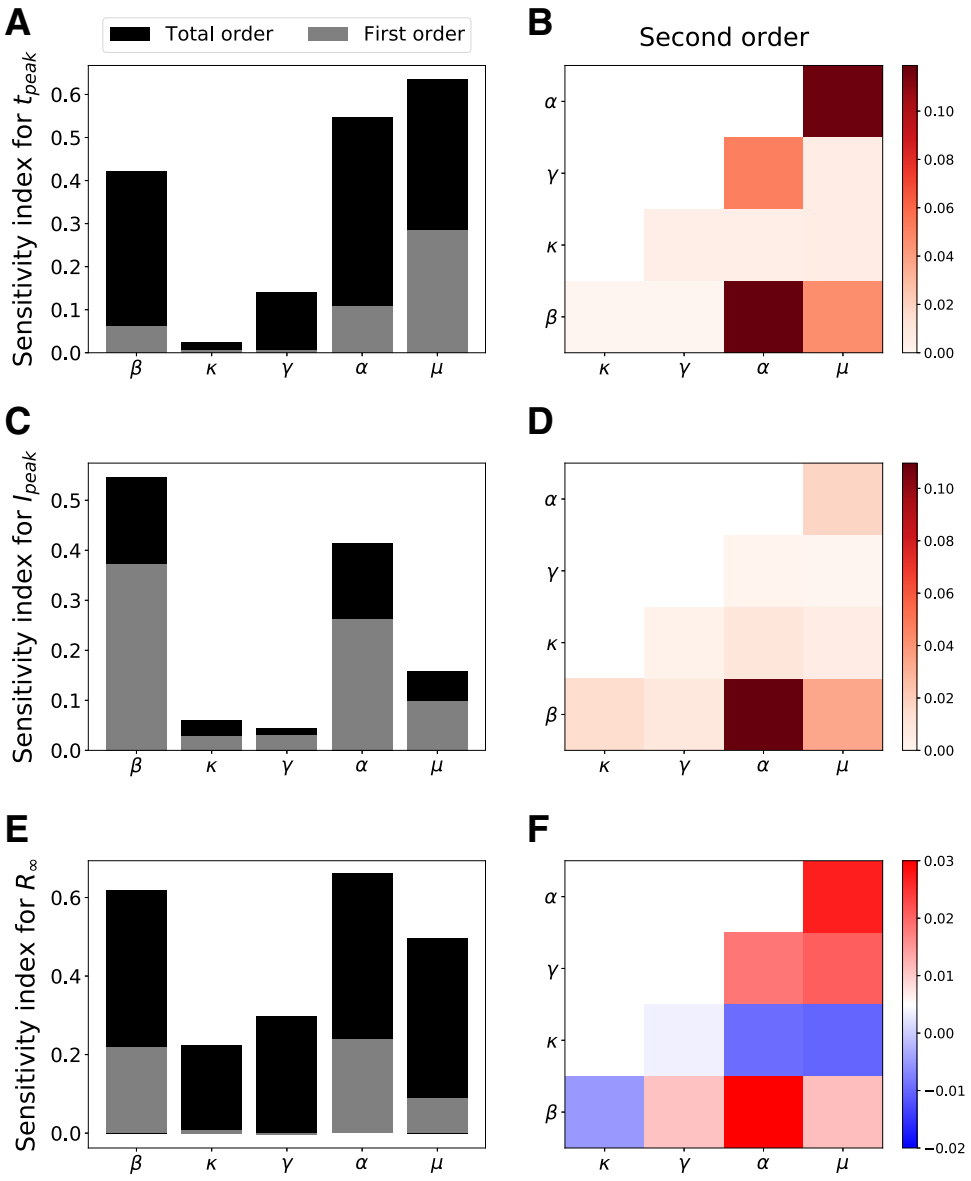

Fig. 6. Global sensitivity analysis of the model parameters performed with the Sobol method with respect to **A and B,** the time at which the infectious population peaks, t_{peak}; **C and D,** the magnitude of this peak, I_{peak}; and **E and F,** the final number of dead hosts, R_∞. A, C, and E show the total and first-order indices, and B, D, and F show the second-order indices.

The fact that the most influential parameters of the model are those related to the vector can be used to design appropriate disease control strategies. Because acting on transmission rates is rather cumbersome, we argue that control strategies should focus on reducing the vector population in crop fields. In our model, this depends on two parameters: μ, the rate at which vectors die (or move to herbaceous vegetation and other non-host trees or exit the field) and $N_v(0)$, the number of newborn susceptible vectors every year (assumed constant in this study). Our results show that a mixed strategy acting on both parameters is optimal to lower disease prevalence and, eventually, eradicate the disease. Interestingly, we also show that acting on the vector removal μ is more effective than controlling the newborn vector population $N_v(0)$. In fact, most control strategies carried out in practice for *X. fastidiosa* diseases focus on the latter factor, reducing $N_v(0)$ via egg or nymph control (Cornara et al. 2018b; Lago et al. 2023; López-Mercadal et al. 2022). However, our results indicate that alternative strategies based on increasing the removal (or dispersal) rate of vectors should be explored. Furthermore, the evolution of the population compartments of the hosts and vectors provides relevant information on the epidemiology of both diseases. In both cases, the newly defined basic reproductive number that accounts for a decaying vector population is very predictive of the moment in which new infections are not produced anymore, coinciding approximately with the peak of infectious hosts. Therefore, any intervention with control measures after this peak would have marginal effects on future disease progression.

Our mathematical model is still rather simple, implementing only a few relevant epidemic processes in contrast to the high complexity of the pathogen−vector−host interactions occurring in plant epidemics. Indeed, the model itself raises some questions about these interactions, for example, whether or not contact rates are homogeneous. Another simplification of the model is the fact that the spatial constraints and the intrinsic stochasticity of the transmission processes are neglected. A straightforward extension of the model would be to include a specific spatial setting and implement the explicit motion of the vector within a stochastic framework, such as individual-based models (Grimm and Railsback 2005). With this, the effectiveness of current and further control strategies could be tested and improve controlling for the motion of the vector. For instance, the control strategy based on the removal of symptomatic trees together with their surrounding trees at a given distance could be implemented in the model, the current effectiveness could be evaluated according to the present protocols, and improved parameters could even be provided to be implemented in the field. Of course, implementing a model in which the spatial degrees of freedom are explicitly represented would require access to further information about vector mobility and spatially resolved data to confront the model, which is not currently available.

Mathematical models tested against experimental data increase our understanding of the system under study. They also help to identify critical parameters that require better prior information to adjust functions relating to different variables and make the model predictions more accurate to suggest and test control strategies (Cunniffe et al. 2015; Jeger et al. 2018). Our mathematical model suggests a certain lack of knowledge of the transmission processes and reveals that the currently available data are not enough to fit complex models dealing with the explicit dynamics of the vector population.

Appendix I

Vector population dynamics

Supplementary Figure S1 shows a time series for the population of *Philaenus spumarius* in Mallorca, taken from López-Mercadal et al. (2021) (in blue). Superimposed (in orange) is the assumption used in our model equation 2, the $\delta(t - nT)$; that is, every year, susceptible vectors appear in the system.

Appendix II

Determination of R_0

The handicap of determining the basic reproductive number of the model equation 2 is that the pre-pandemic fixed point given by $I_H = I_v = 0$ and $S_H = S_H(0)$ is not a fixed point of the system of differential equations because the vector population decays, so the standard methods to compute R_0, such as the next-generation matrix (Diekmann et al. 2010; Giménez-Romero et al. 2022a) do not apply. In Giménez-Romero et al. (2022a), a method was suggested to determine the basic reproductive number in the case of compartmental models of vector-borne transmitted diseases in which the vector population grows or decays. It consists of averaging the instantaneous basic reproductive number over the time of a generation.

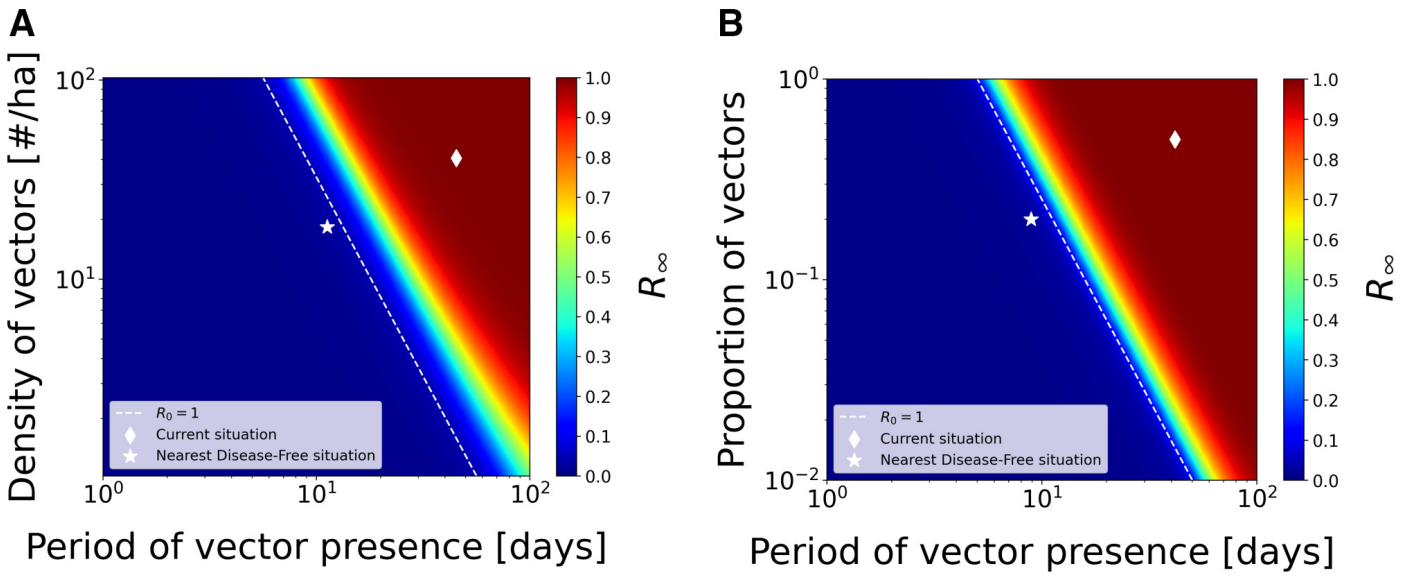

Fig. 7. Epidemic control through vector management for **A,** almond leaf scorch disease in Mallorca and **B,** olive quick decline syndrome in Apulia. The white dashed line denotes $R_0 = 1$, and the white diamond corresponds to the parameter values of the fitted model. The white star is the closest disease-free state to the current situation in this representation.

To proceed, we consider that $I_H = I_v = 0$, $S_H = S_H(0)$ is indeed a fixed point of the system. Then, the basic reproductive number could be determined (e.g., as shown in Brauer et al. 2016). First, an infectious host infects vectors at a rate of $\beta S_H(0)/N_H$ for a time $1/\gamma$. This produces $\beta S_H(0)/\gamma N_H$ infected vectors. The second stage is that these infectious vectors infect hosts at a rate of $\alpha N_v(0)/N_H$ for a time $1/\mu$, producing $\alpha N_v/\mu N_H$ infectious hosts per vector. The net result of these two stages is

$$\tilde{R}_0 = \frac{\alpha\beta}{\mu\gamma}\frac{S_H(0)}{N_H^2}N_v(0) = R_0^* \cdot N_v(0) \quad \text{(i)}$$

This result coincides with the value of R_0 obtained using the standard next-generation matrix method that can be applied in this case because we are assuming that we use a nongeneric initial condition that sits at the fixed point of the model.

In practice, our initial condition will never be a fixed point of the model, and, as mentioned above, we will obtain an approximate basic reproductive number, which we will refer to as R_0 using the method suggested in Giménez-Romero et al. (2022a) that consists of calculating the *average* number of secondary infections produced by an infectious host in one generation. One first defines an instantaneous basic reproductive number,

$$R_0^{(i)}(t) = \frac{\beta\alpha}{\mu\gamma}\frac{S_H(0)}{N_H^2}N_v(t) = R_0^* N_v(t) \quad \text{(ii)}$$

from which the average is simply computed as

$$R_0 = \left\langle R_0^{(i)}(t)\right\rangle\Big|_0^\tau = R_0^* \left\langle N_v(t)\right\rangle\Big|_0^\tau = R_0^* \tfrac{1}{\tau}\int_0^\tau N_v(t)\mathrm{d}t \quad \text{(iii)}$$

In our model, the time-dependent vector population can be obtained from equation 2,

$$\dot{N}_v = \dot{S}_v + \dot{I}_v = -\mu N_v \Rightarrow N_v(t) = N_v(0)\, e^{-\mu t} \quad \text{(iv)}$$

and introducing this expression for $N_v(t)$ in equation iii, the integral can be solved,

$$R_0 = \frac{\beta\alpha S_H(0)}{\mu\gamma N_H^2}\frac{N_v(0)}{\mu\tau}\left(1 - e^{-\mu\tau}\right) = R_0^*\frac{N_v(0)}{\mu\tau}\left(1 - e^{-\mu\tau}\right) \quad \text{(v)}$$

which is an approximated expression to the basic reproductive number for our model in which the vector population is nonstationary, where, in equation ii and equation v, it has been defined, $R_0^* = (\beta\alpha S_H(0))/(\mu\gamma N_H^2)$.

Note that in our model, one generation corresponds to 1 year, and $N_v(0)$ is reset every year.

Literature Cited

Abboud, C., Bonnefon, O., Parent, E., and Soubeyrand, S. 2019. Dating and localizing an invasion from post-introduction data and a coupled reaction–diffusion–absorption model. J. Math. Biol. 79:765-789.

Almeida, R. P. P., and Nunney, L. 1987. How do plant diseases caused by *Xylella fastidiosa* emerge? Plant Dis. 99:1457-1467.

Almeida, R. P. P., and Purcell, A. H. 2003. Biological traits of *Xylella fastidiosa* strains from grapes and almonds. Appl. Environ. Microbiol. 69:7447-7452.

Antonatos, S., Papachristos, D. P., Varikou, K., Vahamidis, P., Kapranas, A., and Milonas, P. 2021. Seasonal appearance, abundance, and host preference of *Philaenus spumarius* and *Neophilaenus campestris* (Hemiptera: Aphrophoridae) in olive groves in Greece. Environ. Entomol. 50:1474-1482.

Bacaër, N. 2007. Approximation of the basic reproduction number R_0 for vector-borne diseases with a periodic vector population. Bull. Math. Biol. 69: 1067-1091.

Beal, D. J., Cooper, M., Daugherty, M. P., Purcell, A. H., and Almeida, R. P. P. 2021. Seasonal abundance and infectivity of *Philaenus spumarius* (Hemiptera: Aphrophoridae), a vector of *Xylella fastidiosa* in California vineyards. Environ. Entomol. 50:467-476.

Bezanson, J., Edelman, A., Karpinski, S., and Shah, V. B. 2017. Julia: A fresh approach to numerical computing. SIAM Rev. 59:65-98.

Bodino, N., Cavalieri, V., Dongiovanni, C., Plazio, E., Saladini, M. A., Volani, S., Simonetto, A., Fumarola, G., Di Carolo, M., Porcelli, F., Gilioli, G., and Bosco, D. 2019. Phenology, seasonal abundance and stage-structure of spittlebug (Hemiptera: Aphrophoridae) populations in olive groves in Italy. Sci. Rep. 9:1-17.

Bodino, N., Cavalieri, V., Pegoraro, M., Altamura, G., Canuto, F., Zicca, S., Fumarola, G., Almeida, R. P. P., Saponari, M., Dongiovanni, C., and Bosco, D. 2021. Temporal dynamics of the transmission of *Xylella fastidiosa* subsp. *pauca* by *Philaenus spumarius* to olive plants. Entomol. Gen. 41:463-480.

Brauer, F., Castillo-Chavez, C., Mubayi, A., and Towers, S. 2016. Some models for epidemics of vector-transmitted diseases. Infect. Dis. Model. 1:79-87.

Brunetti, M., Capasso, V., Montagna, M., and Venturino, E. 2020. A mathematical model for *Xylella fastidiosa* epidemics in the Mediterranean regions. Promoting good agronomic practices for their effective control. Ecol. Modell. 432:109204.

Cavalieri, V., Altamura, G., Fumarola, G., di Carolo, M., Saponari, M., Cornara, D., Bosco, D., and Dongiovanni, C. 2019. Transmission of *Xylella fastidiosa* subspecies *pauca* sequence type 53 by different insect species. Insects 10:324.

Chew, Y. H., Smith, R. W., Jones, H. J., Seaton, D. D., Grima, R., and Halliday, K. J. 2014. Mathematical models light up plant signaling. Plant Cell 26:5-20.

Chiyaka, C., Singer, B. H., Halbert, S. E., Morris, J. G., Jr., and van Bruggen, A. H. C. 2012. Modeling huanglongbing transmission within a citrus tree. Proc. Natl. Acad. Sci. 109:12213-12218.

Chmiel, S. M., and Wilson, M. C. 1979. Estimation of the lower and upper developmental threshold temperatures and duration of the nymphal stages of the meadow spittlebug, *Philaenus spumarius*. Environ. Entomol. 8:682-685.

Chowell, G. 2017. Fitting dynamic models to epidemic outbreaks with quantified uncertainty: A primer for parameter uncertainty, identifiability, and forecasts. Infect. Dis. Model. 2:379-398.

Cornara, D., Bosco, D., and Fereres, A. 2018a. *Philaenus spumarius*: When an old acquaintance becomes a new threat to European agriculture. J. Pest Sci. 91:957-972.

Cornara, D., Cavalieri, V., Dongiovanni, C., Altamura, G., Palmisano, F., Bosco, D., Porcelli, F., Almeida, R. P. P., and Saponari, M. 2017b. Transmission of *Xylella fastidiosa* by naturally infected *Philaenus spumarius* (Hemiptera, Aphrophoridae) to different host plants. J. Appl. Entomol. 141:80-87.

Cornara, D., Garzo, E., Morente, M., Moreno, A., Alba-Tercedor, J., and Fereres, A. 2018b. EPG combined with micro-CT and video recording reveals new insights on the feeding behavior of *Philaenus spumarius*. PLoS One 13: 1-20.

Cornara, D., Panzarino, O., Santoiemma, G., Bodino, N., Loverre, P., Mastronardi, M. G., Mattia, C., De Lillo, E., and Addante, R. 2021. Natural areas as reservoir of candidate vectors of *Xylella fastidiosa*. Bull. Insectol. 74:173-180.

Cornara, D., Saponari, M., Zeilinger, A. R., de Stradis, A., Boscia, D., Loconsole, G., Bosco, D., Martelli, G. P., Almeida, R. P. P., and Porcelli, F. 2017a. Spittlebugs as vectors of *Xylella fastidiosa* in olive orchards in Italy. J. Pest Sci. 90:521-530.

Cunniffe, N. J., Koskella, B., Metcalf, C. J. E., Parnell, S., Gottwald, T. R., and Gilligan, C. A. 2015. Thirteen challenges in modelling plant diseases. Epidemics 10:6-10.

Daugherty, M. P., and Almeida, R. P. P. 2019. Understanding how an invasive vector drives Pierce's disease epidemics: Seasonality and vine-to-vine spread. Phytopathology 109:277-285.

Diekmann, O., Heesterbeek, J. A. P., and Roberts, M. G. 2010. The construction of next-generation matrices for compartmental epidemic models. J. R. Soc. Interface 7:873-885.

Fierro, A., Liccardo, A., and Porcelli, F. 2019. A lattice model to manage the vector and the infection of the *Xylella fastidiosa* on olive trees. Sci. Rep. 9:8723.

Freitag, J. H. 1951. Host range of the Pierce's disease virus of grapes as determined by insect transmission. Phytopathology 41:920-934.

Ge, H., Xu, K., and Ghahramani, Z. 2018. Turing: A language for flexible probabilistic inference. Pages 1682-1690 in: International Conference on Artificial Intelligence and Statistics, AISTATS, Playa Blanca, Lanzarote, Canary Islands, Spain.

Giménez-Romero, À. 2022. A compartmental model for *Xylella fastidiosa* related diseases. GitHub Repo. https://github.com/agimenezromero/A-compartmental-model-for-Xylella-fastidiosa-related-diseases

Giménez-Romero, À., Flaquer-Galmés, R., and Matías, M. A. 2022a. Vector-borne diseases with nonstationary vector populations: The case of growing and decaying populations. Phys. Rev. E 106:054402.

Giménez-Romero, À., Galván, J., Montesinos, M., Bauzà, J., Godefroid, M., Fereres, A., Ramasco, J. J., Matías, M. A., and Moralejo, E. 2022b. Global predictions for the risk of establishment of Pierce's disease of grapevines. Commun. Biol. 5:1389.

Grimm, V., and Railsback, S. F. 2005. Individual-based Modeling and Ecology. Princeton University Press, Princeton, NJ.

Homan, M. D., and Gelman, A. 2014. The no-U-turn sampler: Adaptively setting path lengths in Hamiltonian Monte Carlo. J. Mach. Learn. Res. 15: 1593-1623.

Hopkins, D. L., and Purcell, A. H. 2002. *Xylella fastidiosa*: Cause of Pierce's disease of grapevine and other emergent diseases. Plant Dis. 86:1056-1066.
Jeger, M. J., and Bragard, C. 2019. The epidemiology of *Xylella fastidiosa*; a perspective on current knowledge and framework to investigate plant host-vector-pathogen interactions. Phytopathology 109:200-209.
Jeger, M. J., Holt, J., Van Den Bosch, F., and Madden, L. V. 2004. Epidemiology of insect-transmitted plant viruses: Modelling disease dynamics and control interventions. Physiol. Entomol. 29:291-304.
Jeger, M. J., Madden, L. V., and Van Den Bosch, F. 2018. Plant virus epidemiology: Applications and prospects for mathematical modeling and analysis to improve understanding and disease control. Plant Dis. 102: 837-854.
Jeger, M. J., van den Bosch, F., Madden, L. V., and Holt, J. 1998. A model for analysing plant-virus transmission characteristics and epidemic development. Math. Med. Biol. 15:1-18.
Lago, C., Giménez-Romero, À., Morente, M., Matias, M. A., Moreno, A., and Fereres, A. 2023. Degree-day-based model to predict egg hatching of *Philaenus spumarius* (Hemiptera: Aphrophoridae), the main vector of *Xylella fastidiosa* in Europe. Environ. Entomol. 52:350-359.
Levin, S. A., ed. 1992. Mathematics and Biology: The Interface, Challenges and Opportunities. Lawrence Berkeley Lab, Berkeley, CA.
López-Mercadal, J., Delgado, S., Mercadal, P., Seguí, G., Lalucat, J., Busquets, A., Gomila, M., Lester, K., Kenyon, D. M., Ruiz-Pérez, M., Paredes-Esquivel, C., and Miranda, M. A. 2021. Collection of data and information in Balearic Islands on biology of vectors and potential vectors of *Xylella fastidiosa* (GP/EFSA/ALPHA/017/01). EFSA Supporting Publications 18: 6925E.
López-Mercadal, J., Mercadal-Frontera, P., and Miranda, M. Á. 2022. Mechanical management of weeds drops nymphal density of *Xylella fastidiosa* vectors. bioRxiv 512680.
Madden, L. V., Jeger, M. J., and van den Bosch, F. 2000. A theoretical assessment of the effects of vector-virus transmission mechanism on plant virus disease epidemics. Phytopathology 90:576-594.
Martcheva, M. 2015. An Introduction to Mathematical Epidemiology. Springer, New York.
Moralejo, E., Borras, D., Gomila, M., Montesinos, M., Adrover, F., Juan, A., Nieto, A., Olmo, D., Seguí, G., and Landa, B. B. 2019. Insights into the epidemiology of Pierce's disease in vineyards of Mallorca, Spain. Plant Pathol. 68:1458-1471.
Moralejo, E., Gomila, M., Montesinos, M., Borràs, D., Pascual, A., Nieto, A., Adrover, F., Gost, P. A., Seguí, G., Busquets, A., Jurado-Rivera, J. A., Quetglas, B., García, J. D., Beidas, O., Juan, A., Velasco-Amo, M. P., Landa, B. B., and Olmo, D. 2020. Phylogenetic inference enables reconstruction of a long-overlooked outbreak of almond leaf scorch disease (*Xylella fastidiosa*) in Europe. Commun. Biol. 3:560.
Morente, M., Cornara, D., Plaza, M., Durán, J. M., Capiscol, C., Trillo, R., Ruiz, M., Ruz, C., Sanjuan, S., Pereira, J. A., Moreno, A., and Fereres, A. 2018. Distribution and relative abundance of insect vectors of *Xylella fastidiosa* in olive groves of the Iberian Peninsula. Insects 9:175.
Murray, J. D. 1989. Mathematical Biology. Springer, Berlin, Germany.
Olmo, D., Nieto, A., Borras, D., Montesinos, M., Adrover, F., Pascual, A., Gost, P. A., Quetglas, B., Urbano, A., De Dios Garcia, J., Velasco-Amo, M. P., Olivares-García, C., Beidas, O., Juan, A., Marco-Noales, E., Gomila, M., Rita, J., Moralejo, E., and Landa, B. B. 2021. Landscape epidemiology of *Xylella fastidiosa* in the Balearic Islands. Agronomy 11:473.
Purcell, A. H., and Finlay, A. 1979. Evidence for noncirculative transmission of Pierce's disease bacterium by sharpshooter leafhoppers. Phytopathology 69:393-395.
Rackauckas, C., and Nie, Q. 2017. Differentialequations.jl – A performant and feature-rich ecosystem for solving differential equations in Julia. J. Open Res. Softw. 5:15.
Redak, R. A., Purcell, A. H., Lopes, J. R., Blua, M. J., Mizell, R. F., III, and Andersen, P. C. 2004. The biology of xylem fluid-feeding insect vectors of *Xylella fastidiosa* and their relation to disease epidemiology. Annu. Rev. Entomol. 49:243-270.
Roosa, K., and Chowell, G. 2019. Assessing parameter identifiability in compartmental dynamic models using a computational approach: Application to infectious disease transmission models. Theor. Biol. Med. Modell. 16:1.
Saltelli, A., Tarantola, S., Campolongo, F., and Ratto, M. 2004. Sensitivity Analysis in Practice: A Guide to Assessing Scientific Models. Wiley, Hoboken, NJ.
Saponari, M., Boscia, D., Nigro, F., and Martelli, G. P. 2013. Identification of DNA sequences related to *Xylella fastidiosa* in oleander, almond and olive trees exhibiting leaf scorch symptoms in Apulia (Southern Italy). J. Plant Pathol. 95.
Saponari, M., Giampetruzzi, A., Loconsole, G., Boscia, D., and Saldarelli, P. 2019. *Xylella fastidiosa* in olive in Apulia: Where we stand. Phytopathology 109:175-186.
Sarkar, S., Pressey, R. L., Faith, D. P., Moffett, A., Wilson, K. A., Williams, K. J., Williams, P. H., and Andelman, S. 2006. Biodiversity conservation planning tools. Annu. Rev. Environ. Resour. 31:123-159.
Sobol, I. M. 2001. Global sensitivity indices for nonlinear mathematical models and their Monte Carlo estimates. Math. Comput. Simul 55:271-280.
Soubeyrand, S., de Jerphanion, P., Martin, P., Saussac, M., Manceau, C., Hendrikx, P., and Lannou, C. 2018. Inferring pathogen dynamics from temporal count data: The emergence of *Xylella fastidiosa* in France is probably not recent. New Phytol. 219:824-836.
Stevenson, J. F., Matthews, M. A., Greve, L. C., Labavitch, J. M., and Rost, T. L. 2004. Grapevine susceptibility to Pierce's disease ii: Progression of anatomical symptoms. Am. J. Enol. Vitic. 55:238-245.
Teviotdale, B. L., and Connell, J. H. 2003. Almond Leaf Scorch. ANR University of California, Davis, CA.
Vanhove, M., Retchless, A. C., Sicard, A., Rieux, A., Coletta-Filho, H. D., De La Fuente, L., Stenger, D. C., and Almeida, R. P. P. 2019. Genomic diversity and recombination among *Xylella fastidiosa* subspecies. Appl. Environ. Microbiol. 85:e02972-18.
Virtanen, P., Gommers, R., Oliphant, T. E., Haberland, M., Reddy, T., Cournapeau, D., Burovski, E., Peterson, P., Weckesser, W., Bright, J., van der Walt, S. J., Brett, M., Wilson, J., Millman, K. J., Mayorov, N., Nelson, A. R. J., Jones, E., Kern, R., Larson, E., Carey, C. J., Polat, İ., Feng, Y., Moore, E. W., VanderPlas, J., Laxalde, D., Perktold, J., Cimrman, R., Henriksen, I., Quintero, E. A., Harris, C. R., Archibald, A. M., Ribeiro, A. H., Pedregosa, F., van Mulbregt, P., and SciPy 1.0 Contributors. 2020. SciPy 1.0: Fundamental algorithms for scientific computing in Python. Nat. Methods 17:261-272.
White, S. M., Bullock, J. M., Hooftman, D. A. P., and Chapman, D. S. 2017. Modelling the spread and control of *Xylella fastidiosa* in the early stages of invasion in Apulia, Italy. Biol. Invasions 19:1825-1837.
White, S. M., Navas-Cortés, J. A., Bullock, J. M., Boscia, D., and Chapman, D. S. 2020. Estimating the epidemiology of emerging *Xylella fastidiosa* outbreaks in olives. Plant Pathol. 69:1403-1413.